

ADAPTIVE SCHEMES FOR FEM APPROXIMATION OF THE HIGHER-ORDER GENERALIZED CAHN-HILLIARD EQUATIONS

Emmanuel Y. Medina^a, Bernardo M. Rocha^a and Elson M. Toledo^a

^a*Pós-Graduação em Modelagem Computacional, Universidade Federal de Juiz de Fora, Brasil*
bernardomartinsrocha@ice.ufjf.br, <http://www.ufjf.br/pgmc>

Keywords: Generalized Cahn-Hilliard equation, h-adaptative FEM, higher-order anisotropy, numerical simulation.

Abstract. The Cahn-Hilliard equation was introduced to model the phase separation in two-component alloys. This is one of the mathematical models most used to describe tumor growth through the evolution of healthy, cancerous and dead cells. In this work we present a numerical study of this equation by introducing higher-order derivatives with a nonlinear source term. Our objective is to solve the higher-order anisotropic problem with locally refined meshes in space using the finite element method for the generalized Cahn-Hilliard model. A phenomenological model that can describe the growth of a cancerous tumor will be treated. Numerical simulations are presented to illustrate the effects of higher-order terms on anisotropy and studies with space adaptivity strategy are also presented indicating its computational efficiency when compared to fixed meshes, especially in the case of anisotropic problems.

1 INTRODUCTION

Phase-field models have rapidly gained popularity over the last twenty years in various fields, and examples of their applications have been studied in the formation of microstructures during solidification, in solid-state transformations (Chen, 2002; Wang and Li, 2010); in multiphase flows (Anderson et al., 1998) as it can be seen in the recent reviews (Boettinger et al., 2002; Plapp, 2007). The number of application areas treated with the help of phase-field models is large, since this is a rapidly advancing field. All these areas have in common the fact that they involve the motion of interfaces or boundaries in response to a coupling of the boundary with one or several transport fields (such as diffusion, flow, stress or temperature fields). This interaction generates morphological instabilities and leads to the spontaneous emergence of complex structures.

In the context of materials sciences the classical Cahn-Hilliard (CH) equation describes important qualitative features of two-phase systems related with phase separation processes, where isotropy and constant temperature are assumed. The application of this model in cases involving phase separations allows to capture the dynamics of a fast initial separation, resulting in the formation of a diffuse interface between the two phases of the mixtures. Then, at a second stage, in a slower time scale diffusion occurs to define the phases. These two stages are characterized by dynamics in different time and space scales, which makes the numerical solution of the Cahn-Hilliard equation difficult. For more details on applications we refer the reader to Cahn and Hilliard (1958); Cahn (1961); Cherfils et al. (2011); Langer (1971) and Maier-Paape and Wanner (2000) for more details.

One of the applications of phase field modeling is in the modeling of cancer diseases. Hana-han and Weinberg (2011) describe a set of characteristics for the formation of tumor cells. Byrne et al. (1999) address possible effective treatments for the disease, where the knowledge of the mechanisms of growth and interaction between tumor cells are relevant for a possible eradication of the disease. In this context, mathematical and computational modeling can support research on this area through development of models that describe the different aspects of tumor growth and which allows new types of experimentation and understanding.

The use of Cahn-Hilliard type equations in biological modeling is somewhat recent. The earliest work in this context was written by Cohen and Murray (1981), where they essentially reintroduced the Cahn-Hilliard equation in the setting of ecological population dynamics and added a source term to model the growth of the population. Their main motivation was that the Fickian diffusion model, which is used quite frequently in ecological equations, is too restrictive in many cases. They gave the example of populations that exhibit negative diffusion, in other words, populations that tend to aggregate. The Cahn-Hilliard diffusion operator, though nonlinear, is general enough to describe backward diffusion and Fickian diffusion as special cases.

Cristini et al. (2008) and Wise et al. (2008) presented Cahn-Hilliard models in the context of cancerous tumour growth. These models are rather complicated and include several variables. Their source terms are essentially composed of a part that accounts for cell mitosis (growth) and for cell apoptosis and necrosis (cell death). The CH model can be viewed as a simplified version of the models studied in Cristini et al. (2008) and Wise et al. (2008) (without considering the anisotropic terms of the high order coefficients), being one that yields qualitatively comparable model predictions in some sense. Hawkins-Daarud et al. (2012) presented a four-species model of tumor growth based on the Cahn-Hilliard/diffuse-interface framework and a mixed (continuous) finite element framework (unconditionally gradient stable, first-order accurate in time and

mass conservative) was used to numerically solve it.

In the simulations of anisotropic higher-order Cahn-Hilliard equations, the resulting growth from the source term increases the need for a high spatial resolution of the finite element mesh to correctly resolve the growth of the sharp interface region. Simulations with meshes with a large number of nodes are computationally expensive as it requires repeated solutions of large scale linear systems. In addition, the fine time steps required for accurate and stable simulations (Eyre, 1998) poses an even more challenging computational problem. Therefore, the use of adaptive mesh methods provides a solution to overcome these problems. The adaptive mesh algorithm works to maintain a fine resolution only where it is needed (i.e., near the sharp interface that is growing) so that the number of degrees of freedom is significantly reduced, resulting in more efficient computations while at the same time capturing the correct dynamics of growth. In this work we introduce the use of an adaptive mesh algorithm in the solution to the anisotropic higher-order Cahn-Hilliard equation for tumor growth.

This paper is organized as follows: the model problem is presented in Section 2. In Section 3 the numerical formulation based on mixed finite elements and the time discretization scheme for this problem is recalled. The mesh adaptivity algorithm employed in this work is also presented. Numerical results are presented in Section 4 for different anisotropy scenarios. Comparisons between solutions obtained with fixed and adaptive meshes are presented in terms of computational performance illustrating the potential of the proposed formulation to simulate efficiently the higher-order Cahn-Hilliard equations for modeling tumor growth. Concluding remarks are mentioned in Section 5.

2 MATHEMATICAL MODEL

The classical Cahn-Hilliard equation is defined by

$$\frac{\partial u}{\partial t} + \Delta^2 u - \Delta \frac{1}{\epsilon} f(u) + \frac{1}{\epsilon} g(\mathbf{x}, u) = 0, \quad \text{in } \Omega, \quad (1)$$

where Ω is a two-dimensional domain, $\mathbf{x} = \{x, y\}$ denotes the spatial coordinates, $\Delta(\cdot)$ is the laplacian operator, u represents the variable of interest in the range $[-1, 1]$ where $u \approx 1$ indicates a saturation of tumor cells and $u \approx -1$ indicates a saturation of healthy cells. Here, $\epsilon > 0$ is a parameter relative to the interface between the components, $f(u)$ is the derivative of $F(\cdot)$ which is the free energy in a homogeneous system and $g(\mathbf{x}, u)$ is a volumetric source term. This source term can be used to describe the growth of cancerous tumours and other biological entities. In this case, when $g(x, u) \neq 0$, the mass can change in time, and the energy defined above can possibly increase. The following free energy $F(u)$ function

$$F(u) = \frac{1}{4}(u^2 - 1)^2, \quad (2)$$

which has the form of a double well is usually employed for CH models was considered in this work.

To describe the growth of the cancerous tumor we consider a nonlinear sixth-order parabolic partial differential equation (Cherfils et al., 2017; Wise et al., 2008). The model is given by:

$$\frac{\partial u}{\partial t} - \Delta \mathcal{A}u + \Delta \mathcal{B}u - \Delta \frac{1}{\epsilon} f(u) + \frac{1}{\epsilon} g(x, u) = 0, \quad \text{in } \Omega, \quad (3)$$

subject to initial conditions $u(\mathbf{x}, 0) = u_0$ and periodic boundary conditions. Here, \mathcal{A} and \mathcal{B} are operators defined by:

$$\mathcal{A} = a_{20}\epsilon \frac{\partial^4}{\partial x^4} + a_{02}\epsilon \frac{\partial^4}{\partial y^4} + a_{11}\epsilon \frac{\partial^4}{\partial x^2 \partial y^2}, \quad (4)$$

$$\mathcal{B} = a_{10}\epsilon \frac{\partial^2}{\partial x^2} + a_{01}\epsilon \frac{\partial^2}{\partial y^2}. \quad (5)$$

Note that in the case of $a_{20} = a_{02} = a_{11} = 0$ the equation (3) reduces to the classical Cahn-Hilliard equation (3). A detailed analysis of the solution for equation (3) was presented by [Cherifils et al. \(2017\)](#) and [Miranville \(2013\)](#).

In equation (3) the source term $g(\mathbf{x}, u)$ acts as a proliferation term, as proposed by [Khain and Sander \(2008\)](#), in view of biological applications. In this work we choose $g(\mathbf{x}, u)$ as follows:

$$g(\mathbf{x}, u) = m_d(u + 1) - m_g(1 - u)^2(1 + u)^2,$$

which was proposed by [Aristotelous et al., 2015](#)) for tumor growth, where m_d and m_g are death and growth coefficients constants, respectively.

We focus here on the anisotropic case with sixth-order partial derivatives, which influences the pattern of tumor growth. For instance, when $a_{20} > a_{02}$ and $a_{20} > a_{11}$ there is an anisotropic behavior, where a differentiated pattern in the x -direction is obtained. In the case where $a_{02} > a_{20}$ and $a_{02} > a_{11}$ the pattern of tumor growth will be predominant in the y -direction, and in the case where $a_{11} > a_{20}$ and $a_{11} > a_{02}$ a complex pattern, called cross anisotropy, which acts in both directions x and y is observed.

3 NUMERICAL FORMULATION

The numerical scheme adopted in this work to solve the higher-order Cahn-Hilliard equation (3) employs a mixed finite element formulation for the spatial discretization and the backward Euler method combined with the [Eyre \(1998\)](#) scheme for the time discretization. To correctly capture the growth dynamics without the use of highly refined mesh resolution, we employ an adaptive mesh algorithm for the finite element formulation. Before, introducing the numerical methods, basic notation is introduced. We consider $V^h \subseteq H_{per}^1$ the following finite element space

$$V^h = \{z \in C^0(\bar{\Omega}) : z|_{\tau} \in \mathbb{P}_k(\tau), \tau \in \mathcal{T}^h, z|_{\partial\Omega} \text{ periodic}\}, \quad (6)$$

where \mathcal{T}^h is a family of triangulations of the domain Ω and \mathbb{P}_k denotes the set of polynomials of degree less than or equal to k . In this work we only considered the linear case with $k = 1$ to obtain discrete approximations u_h of u . The time domain is equally split into n time steps $\Delta t_n = t_{n+1} - t_n$, which is denoted by $\Delta t_n = \Delta t$ for simplicity.

3.1 Mixed variational formulation

Before introducing the mixed variational formulation the equation (3) is rewritten by introducing a new variable $v = -\mathcal{A}u - \mathcal{B}u - \frac{1}{\epsilon}f(u)$ to obtain the following mixed problem:

$$\frac{\partial u}{\partial t} + \Delta v + g(\mathbf{x}, u) = 0, \quad (7)$$

$$v + a_{20}\epsilon \frac{\partial^4 u}{\partial x^4} + a_{02}\epsilon \frac{\partial^4 u}{\partial y^4} + a_{11}\epsilon \frac{\partial^4 u}{\partial x^2 \partial y^2} - a_{10}\epsilon \frac{\partial^2 u}{\partial x^2} - a_{01}\epsilon \frac{\partial^2 u}{\partial y^2} + \frac{1}{\epsilon}f(u) = 0. \quad (8)$$

Additionally, the following variables are introduced

$$\frac{\partial^2 u}{\partial x^2} = p, \quad \frac{\partial^2 u}{\partial y^2} = q, \tag{9}$$

such that

$$\frac{\partial^4 u}{\partial x^2 \partial y^2} = \frac{1}{2} \frac{\partial^2 p}{\partial y^2} + \frac{1}{2} \frac{\partial^2 q}{\partial x^2}. \tag{10}$$

Then, the following variational formulation is presented: find $(u, v, p, q) \in H_{per}^1(\Omega)^4$ such that

$$\left(\frac{\partial u}{\partial t}, v_1\right) - (\nabla v, \nabla v_1) + \frac{1}{\epsilon}(g(\mathbf{x}, u), v_1) = 0, \tag{11}$$

$$\begin{aligned} (v, v_2) - a_{20}\epsilon \left(\frac{\partial p}{\partial x}, \frac{\partial v_2}{\partial x}\right) - a_{02}\epsilon \left(\frac{\partial q}{\partial y}, \frac{\partial v_2}{\partial y}\right) - \frac{a_{11}\epsilon}{2} \left(\frac{\partial q}{\partial x}, \frac{\partial v_2}{\partial x}\right) \\ - \frac{a_{11}\epsilon}{2} \left(\frac{\partial p}{\partial y}, \frac{\partial v_2}{\partial y}\right) - a_{10}\epsilon(p, v_2) - a_{01}\epsilon(q, v_2) + \frac{1}{\epsilon}(f(u), v_2) = 0, \end{aligned} \tag{12}$$

$$(p, v_3) + \left(\frac{\partial u}{\partial x}, \frac{\partial v_3}{\partial x}\right) = 0, \tag{13}$$

$$(q, v_4) + \left(\frac{\partial u}{\partial y}, \frac{\partial v_4}{\partial y}\right) = 0, \tag{14}$$

for all v_1, v_2, v_3, v_4 in V^h and where $(w, z) = \int_{\Omega} w z d\Omega$ denotes the $L^2(\Omega)$ inner product.

3.2 Time integration

Next we introduce the implicit Euler method for time discretization of equation (11). The resulting fully discrete problem is given by:

$$\left(\frac{u^{n+1}-u^n}{\Delta t}, v_1\right) - (\nabla v^{n+1}, \nabla v_1) + \frac{1}{\epsilon}(g(\mathbf{x}, u^{n+1}), v_1) = 0, \tag{15}$$

$$\begin{aligned} (v^{n+1}, v_2) - a_{20}\epsilon \left(\frac{\partial p^{n+1}}{\partial x}, \frac{\partial v_2}{\partial x}\right) - a_{02}\epsilon \left(\frac{\partial q^{n+1}}{\partial y}, \frac{\partial v_2}{\partial y}\right) - \frac{a_{11}\epsilon}{2} \left(\frac{\partial q^{n+1}}{\partial x}, \frac{\partial v_2}{\partial x}\right) \\ - \frac{a_{11}\epsilon}{2} \left(\frac{\partial p^{n+1}}{\partial y}, \frac{\partial v_2}{\partial y}\right) - a_{10}\epsilon(p^{n+1}, v_2) - a_{01}\epsilon(q^{n+1}, v_2) + \frac{1}{\epsilon}(f(u^{n+1}), v_2) = 0, \end{aligned} \tag{16}$$

$$(p^{n+1}, v_3) + \left(\frac{\partial u^{n+1}}{\partial x}, \frac{\partial v_3}{\partial x}\right) = 0, \tag{17}$$

$$(q^{n+1}, v_4) + \left(\frac{\partial u^{n+1}}{\partial y}, \frac{\partial v_4}{\partial y}\right) = 0, \tag{18}$$

for all test functions v_1, v_2, v_3, v_4 in V^h .

Note that due to the presence of the nonlinear term $f(u^{n+1})$ this scheme would require the solution of a coupled nonlinear system of equations. In this work we adopt the semi-implicit scheme proposed by [Eyre \(1998\)](#) to solve the higher-order Cahn-Hilliard equation. This scheme is unconditionally stable by using a convex-concave splitting of $f(u)$ in the following form

$$f(u) = f_c(u) + f_e(u), \tag{19}$$

where the convex part $f_c(u)$ is treated implicitly, whereas the concave part $f_e(u)$ is explicit in time. Note that these choices are not unique and in this paper we considered the following functions: $f_c(u) = 2u$ and $f_e(u) = u^3 - 3u$.

However, the source term $g(u)$ could be also nonlinear, as is the case in this work. Therefore, the next step is to make use of the Picard iterative method for the treatment of the nonlinear term $g(u)$. In this context we denote by u_k^{n+1} the approximate solution to be found at time instant

t^{n+1} at step k of the Picard method. Thus, the following set of equations have to be solved by iteration:

$$\left(\frac{u_{k+1}^{n+1} - u^n}{\Delta t}, v_1 \right) - (\nabla v_{k+1}^{n+1}, \nabla v_1) + (g(u_k^{n+1}), v_1) = 0, \quad (20)$$

$$\begin{aligned} (v_{k+1}^{n+1}, v_2) - a_{20}\epsilon \left(\frac{\partial p_{k+1}^{n+1}}{\partial x}, v_2 \right) - a_{02}\epsilon \left(\frac{\partial q_{k+1}^{n+1}}{\partial y}, v_2 \right) \\ - \frac{a_{11}\epsilon}{2} \left(\frac{\partial q_{k+1}^{n+1}}{\partial x}, \frac{\partial v_2}{\partial x} \right) - \frac{a_{11}\epsilon}{2} \left(\frac{\partial p_{k+1}^{n+1}}{\partial y}, \frac{\partial v_2}{\partial y} \right) \\ - a_{10}\epsilon (p_{k+1}^{n+1}, v_2) - a_{01}\epsilon (q_{k+1}^{n+1}, v_2) \\ + \frac{1}{\epsilon} (f_c(u_{k+1}^{n+1}) + f_e(u^n, v_2)) = 0, \end{aligned} \quad (21)$$

$$(p_{k+1}^{n+1}, v_3) + \left(\frac{\partial u_{k+1}^{n+1}}{\partial x}, \frac{\partial v_3}{\partial x} \right) = 0, \quad (22)$$

$$(q_{k+1}^{n+1}, v_4) + \left(\frac{\partial u_{k+1}^{n+1}}{\partial y}, \frac{\partial v_4}{\partial y} \right) = 0. \quad (23)$$

The solution algorithm to obtain approximated solutions for the higher-order Cahn-Hilliard equations is described in Algorithm 1.

Algorithm 1: Solution of the higher-order Cahn-Hilliard equations.

```

1 Input:  $u^0, \Delta t, T, k_{\max}, \text{tol}$ ;
2 Output:  $u^{n+1}, v^{n+1}, p^{n+1}, q^{n+1}$ ;
3  $n \leftarrow 0$ ;
4 while  $n\Delta t \leq T$  do
5    $u_0^{n+1} \leftarrow u^n$ ;
6    $k \leftarrow 0$ ;
7   while  $k < k_{\max}$  do
8     find:  $u_{k+1}^{n+1}, v_{k+1}^{n+1}, p_{k+1}^{n+1}, q_{k+1}^{n+1}$ , in eqs. (16 – 19) given  $u^n, u_k^{n+1}$ ;
9     if  $\max |u_{k+1}^{n+1} - u_k^{n+1}| < \text{tol}$  then break;
10     $k \leftarrow k + 1$ ;
11  end
12   $u^{n+1} \leftarrow u_{k+1}^{n+1}$ ;
13   $n \leftarrow n + 1$ ;
14 end

```

3.3 Mesh adaptivity

In this work we explore the effects and performance of the solution by considering an adaptive mesh algorithm for higher-order Cahn-Hilliard equations. To this end, we used the mesh adaptation algorithm from FreeFem++ (Hecht, 1998, 2012) in which a variable metric/Delaunay automatic meshing algorithm is implemented. The essential idea is to redefine the scalar product used in an automatic mesh generator to evaluate distance and volume, to construct equilateral elements according to a new adequate metric. The procedure is briefly described next.

The mesh adaptation is based on the Delaunay-Voronoi algorithm considering a specified distance function for two points. Thus, for a distance (or metric) matrix \mathcal{M} the associated distance $d(x, y)$ is

$$d(x, y) = \|x - y\|, \quad \text{where} \quad \|x\|^2 = x^T M x. \quad (24)$$

Thus, the length $l_{\mathcal{M}}$ of a curve $\gamma \in]0, 1[$ with respect to \mathcal{M} is given by:

$$l_{\mathcal{M}} = \int_0^1 \sqrt{\gamma'(t)\mathcal{M}(\gamma(t))\gamma'(t)} dt \tag{25}$$

There are some options to compute \mathcal{M} , as discussed in Hecht (2012). However, in this work the scalar product is based on the evaluation of the Hessian of the variable u of the problem. For P_1 continuous finite elements the metric can be defined by

$$l_{\mathcal{M}} = \frac{1}{err} |\partial_h^2 u_h|, \tag{26}$$

where $|\partial_h^2 u_h| = \sqrt{(|\partial_h^2 u_h|)^2}$ and $\partial_h^2 u_h$ is an approximation of the Hessian matrix of u_h , which is done automatically by FreeFem++ by default. The adaptive algorithm is implemented by the `adaptmesh` function, which in this work was used with the following parameters:

```
Th = adaptmesh(Th, u, hmin=0.0001, hmax=0.05, nbvx=22e5,
              periodic=[[1,x],[3,x],[2,y],[4,y]]),
```

where `Th` is the finite element mesh; `u` is the variable of interest; `hmin` is the minimum edge size; `nbvx` is the maximum number of vertices and `periodic` defines the boundary conditions of the problem. In addition, we remark that the simulations were carried out with an initial grid resolution of 100×100 triangular elements to properly capture the initial conditions.

4 NUMERICAL EXPERIMENTS

In this section we present some numerical simulations to illustrate the effects of anisotropic higher-order terms on CH dynamics and mesh adaptivity. All the computations presented were performed with the finite element library FreeFem++ (Hecht, 1998, 2012) and considered a two-dimensional mesh of triangular elements. We also carried out simulations for fixed and adaptive meshes to compare the results and computational performance.

4.1 Problem settings

To consider avascular tumor growth, numerical experiments are performed for the higher-order Cahn-Hilliard equation with a mass source (proliferation term) for tumor growth. Equation (3) was considered with the following set of parameters as described by (Cherfils et al., 2017):

$$\Omega = (-0.7, 1.7) \times (-1.7, 0.7), \quad \Delta t = 1 \times 10^{-6}, \quad \epsilon = 0.0125, \tag{27}$$

$$f(u) = u^3 - u, \quad g(x, u) = 46u(1 + u) + 280(u - 1)^2(u + 1)^2, \tag{28}$$

and the following initial condition

$$u_0(x, y, 0) = -\tanh\left(\frac{1}{\sqrt{2}\epsilon} \left(\sqrt{2(x - 0.5)^2 + 0.25(y + 0.5)^2} - 0.1\right)\right). \tag{29}$$

which prescribes an initial mass of tumor in the center of the domain. The Table 1 presents a summary of the parameters used for the classical CH and anisotropic higher-order CH cases used in the simulations.

Table 1: Coefficients a_{ij} used in the simulations.

Case	a_{20}	a_{02}	a_{11}	a_{10}	a_{01}
Cahn-Hilliard	0	0	0	1	1
x -direction	1.8×10^{-5}	5.0×10^{-6}	5.0×10^{-6}	1	1
y -direction	5.0×10^{-6}	1.8×10^{-5}	5.0×10^{-6}	1	1
cross-direction	5.0×10^{-6}	5.0×10^{-6}	1.8×10^{-5}	1	1

4.2 Cahn-Hilliard solution

Initially, in Figure 1 we show the results of a tumor growth simulated with the classical Cahn-Hilliard model, where the parameters were taken from the first row of Table 1. In this case the adaptive approximation of the solution is shown, where the spatial distribution of the density of u indicates: $u \approx 1$ (dark red color) a saturation of tumour cells, $u \approx -1$ (light blue color) indicates no tumour cells and $u \approx 0$ shows the diffusive interface between tumor cells and healthy cells.

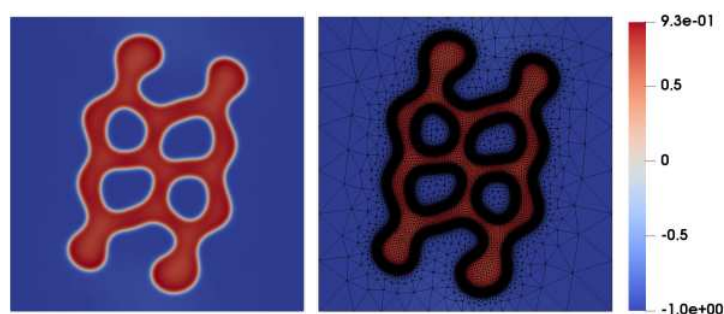


Figure 1: Solution of the Cahn-Hilliard equation using adaptive mesh with 16325 triangular elements. Shown are filled contour plots of the density u and final adaptive mesh.

4.3 Fixed mesh comparison

First we present results for the cross anisotropic case, as described in Table 1, comparing the dynamics of the solution between fixed and adaptive mesh cases. Fixed triangular meshes were created by subdividing the square domain using $(N_x + 1) \times (N_y + 1)$ nodes in each direction, thus resulting in a structured finite element mesh comprised of a total of $N_x \times N_y \times 2$ elements. For instance, in the case $N_x = N_y = 300$, to ease the notation the fixed mesh cases will be simply referred as to 300×300 . The fixed mesh solutions considered in the experiments were: 100×100 , 150×150 , 200×200 , 300×300 and 400×400 . For these cases the discretizations resulted in a total of 20000, 450000, 80000, 180000 and 320000 triangular elements, respectively.

Fig. 2 show the contour plot of the solution u with fixed uniform meshes and adaptive meshing. We observe that the adaptive mesh takes the same shape of the corresponding solution with fixed mesh for (the cases of 300×300 and 400×400 triangular elements).

The profiles of the solutions obtained with different discretizations and adaptive mesh are compared at a diagonal line starting from $(-0.7, -1.7)$ to $(1.7, 0.7)$ in Figure 3. The results show that coarse discretizations, up to 250×250 triangular elements, fail to correctly capture the generated pattern, whereas the refined meshes starting from 300×300 approximate to the

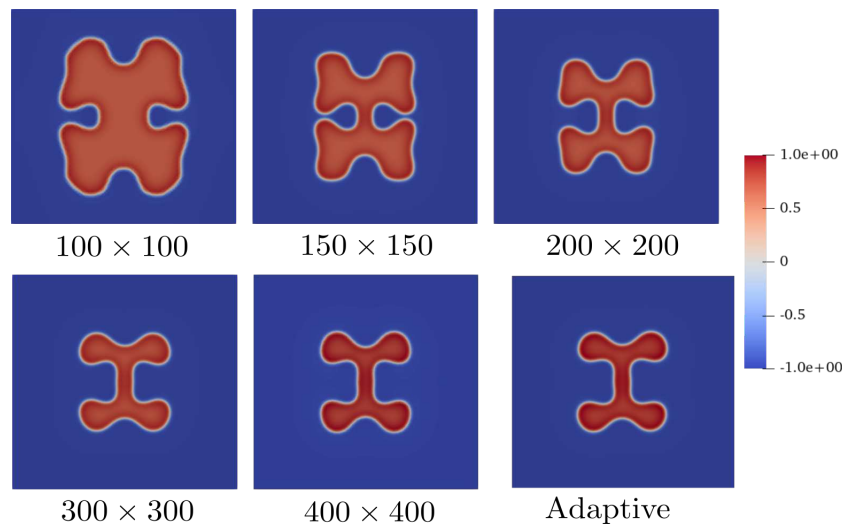


Figure 2: Comparison of the solution u at time instant $t = 1.3 \times 10^{-2}$ using fixed meshes with 100×100 , 150×150 , 200×200 and 300×300 triangular elements and adaptive mesh for the case of cross anisotropy with 23568 triangular elements.

same solution. Therefore, we considered the fixed mesh of 300×300 elements as a reference case. In this scenario efficient computational performance is achieved, since we would have to employ, at least, exactly 180000 triangles for the reference fixed mesh case, whereas for the adaptive mesh we used no more than about a maximum 45000 triangles, as shall be discussed next.

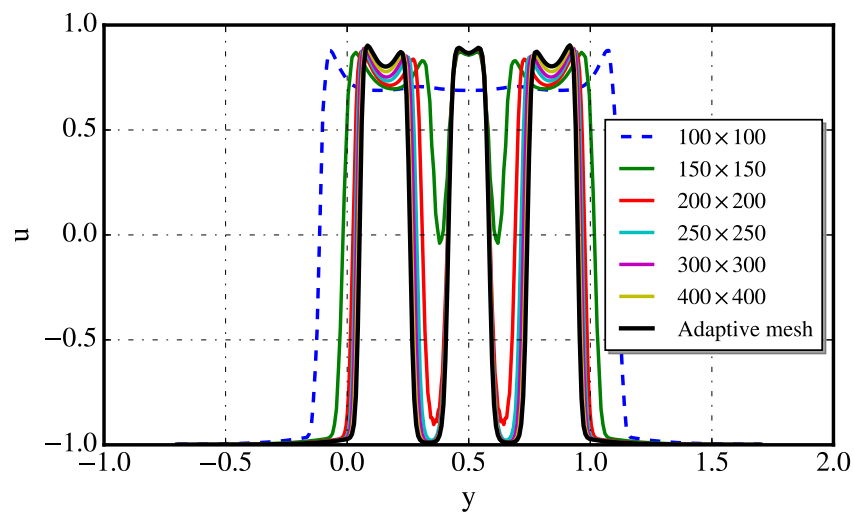


Figure 3: Comparison of the solutions at a diagonal line in the domain for the different fixed mesh cases and the adaptive mesh strategy.

4.4 Effects of anisotropy

With very small coefficients for the sixth-order terms a_{20} , a_{02} and a_{11} , the tumor growth evolves similarly, although the x , y and cross directions are clearly more influenced, as shown in Figure 4, on panels (a), (b) and (c), respectively. Here, we can notice that the tumor mass first

elongates in the x -direction and then grows into a more complicated structure as time evolves. Analogously for the cases with anisotropy in y -direction (cross-direction), the tumor mass firsts elongates in the y -direction (cross-direction) and, then, grows into a more complicated pattern. The results show that the anisotropy is strongly influenced by the choice of the coefficients in the higher-order terms.

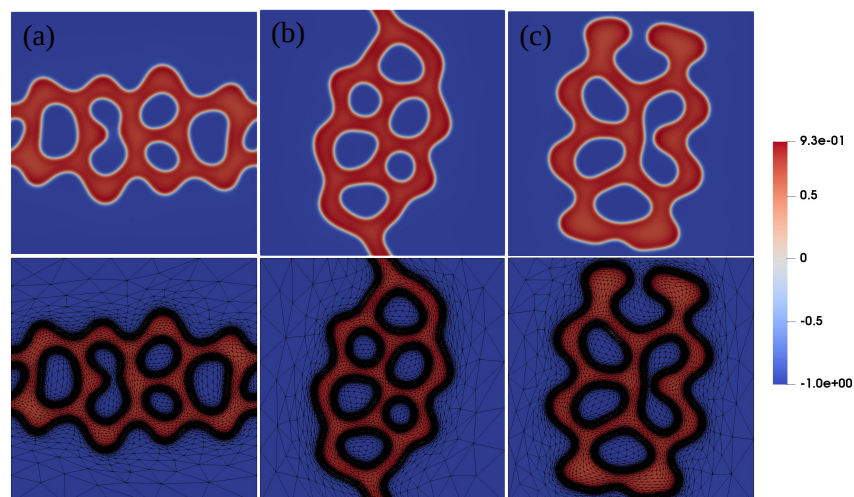


Figure 4: Solutions of the anisotropic cases at time instant $t = 2.0 \times 10^{-2}$: (a) x direction with 22592 elements; (b) y direction with 20482 elements; (c) and cross direction with 29750 elements.

This complex growth phenomenon occurs because there is a strong mass source at the boundary of the tumor where the tumor (dark region) meets the healthy tissue (light region) and a mass sink in the interior of the tumor domain. The mass source is biologically related to cell division and growth and the mass sink is related to the cell death due to hypoxia and necrosis. A detailed description of this behavior is complicated and occurs essentially due to diffusion instability; see [Cristini et al. \(2008\)](#) and [Wise et al. \(2008\)](#) for further details.

4.5 Computational performance

Next, considering the adaptive mesh scheme with $h_{\min}=0.0001$ and $h_{\max}=0.05$ and starting with an initial mesh of 100×100 triangular elements, we studied the remeshing during the entire simulation of the dynamics of tumor growth in the anisotropic case until $t = 2.5 \times 10^{-2}$ in terms of the number of elements. Figure 5 shows the number of triangular elements used in the adaptive mesh algorithm for each time instant of the numerical simulation for the classical Cahn-Hilliard and the anisotropic cases presented before, which were detailed in Table 1.

Note that for the cross-direction the number of elements was higher than the other cases, since the dynamics is more complex. Also note that the pattern of anisotropic growth for the x -direction is more complex than in the y -direction, as can be seen in panels (a) and (b) from Figure 4, which resulted in more elements for the x -direction case.

Finally, when comparing the adaptive mesh scheme with the fixed mesh scheme with $300 \times 300 \times 2$ triangular elements at the time $t = 2, 5 \times 10^{-2}$, we can see that the adaptive mesh scheme always used less elements, no more than 45000 elements, and therefore, was more efficient in terms of computational resources.

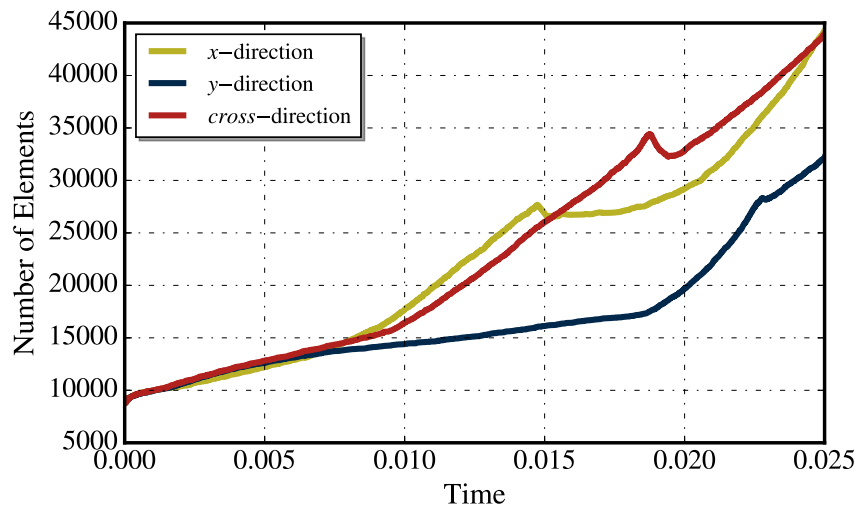


Figure 5: Number of triangular elements for the adaptive mesh simulation as a function of time for the x , y and cross directions anisotropic cases.

5 DISCUSSION

The adaptive mesh algorithm depends on a set of parameters such as the values of the minimum and maximum edge size, maximum number of vertices and initial mesh resolution. In this work after an initial evaluation of the parameters, a specific setting which resulted in successful simulations, as reported in section 4.3 and Figure 2, was found and their values were kept fixed. In future works the effects of `hmin` and `hmax` could be further explored to further improve the computational performance without compromising the quality of the numerical approximations.

Additionally, we remark that the choice of the initial resolution for the adaptive mesh algorithm is important and should be evaluated with care, since in our initial experiments a very coarse mesh significantly affected the obtained pattern in the end of the simulations since it was not able to capture the proper initial conditions.

With respect to related works, we remark that adaptive mesh schemes have been used with success in the context of Cahn–Hilliard equations. Spatially adaptive simulations were performed in Wise et al. (2011) and Hawkins-Daarud et al. (2012). A more detailed analysis was presented in Aristotelous et al. (2015) using a discontinuous Galerkin method and a marking strategy based on an inverse estimate which indicates if the solution at the element is highly oscillatory and should be refined. In particular Han and Wang (2015) presented an adaptive algorithm for the CH equation coupled to the Navier-Stokes equations. The adaptive mesh algorithm used was the same as presented here based on FreeFem++ (Hecht, 2012) and its adaptive meshing. Considering the importance and practical use of adaptive algorithms for CH models, we remark that to the best of our knowledge the present work is the first that considers adaptivity for the high-order anisotropic CH equation.

6 CONCLUSIONS

In this work we presented an adaptive mesh algorithm for the efficient and proper numerical solution of the anisotropic higher-order Cahn-Hilliard equation with a proliferation term. The numerical solution was performed using a mixed finite element method for spatial discretization. For time integration the implicit Euler combined with the Eyre scheme, for the treatment

of the nonlinear term, was employed.

The results of this work showed that the adaptive mesh scheme was able to reproduce the dynamics of tumor growth when compared to a very spatially refined mesh. In addition, the numerical experiments have shown that the total number of elements for the adaptive case is lower than in the refined reference solution most of the time during the simulation, resulting in a considerable gain in computational economy. For instance, we observed that for the fixed mesh at least 180000 triangles had to be used in the spatial discretization. For the adaptive mesh we used no more than 45000 triangles to reproduce the same dynamics of the tumour growth driven by diffusion instability.

ACKNOWLEDGEMENTS

This study was financed in part by the Coordenação de Aperfeiçoamento de Pessoal de Nível Superior - Brasil (CAPES) - Finance Code 001, FAPEMIG, CNPq and UFJF.

REFERENCES

- Anderson D.M., McFadden G.B., and Wheeler A.A. Diffuse-interface methods in fluid mechanics. *Annual review of fluid mechanics*, 30(1):139–165, 1998.
- Aristotelous A.C., Karakashian O.A., and Wise S.M. Adaptive, second-order in time, primitive-variable discontinuous Galerkin schemes for a Cahn–Hilliard equation with a mass source. *IMA Journal of Numerical Analysis*, 35(3):1167–1198, 2015.
- Boettinger W.J., Warren J.A., Beckermann C., and Karma A. Phase-field simulation of solidification. *Annual review of materials research*, 32(1):163–194, 2002.
- Byrne H. et al. Using mathematics to study solid tumour growth. In *Proceedings of the 9th General Meetings of European Women in Mathematics*, pages 81–107. New York: Hindawi Publishing, 1999.
- Cahn J.W. On spinodal decomposition. *Acta Metallurgica*, 9(9):795–801, 1961.
- Cahn J.W. and Hilliard J.E. Free energy of a nonuniform system. I. interfacial free energy. *The Journal of Chemical Physics*, 28(2):258–267, 1958.
- Chen L.Q. Phase-field models for microstructure evolution. *Annual Review of Materials Research*, 32(1):113–140, 2002.
- Cherfils L., Miranville A., Peng S., and Zhang W. Higher-order generalized Cahn–Hilliard equations. *Electronic Journal of Qualitative Theory of Differential Equations*, 2017(9):1–22, 2017.
- Cherfils L., Miranville A., and Zelik S. The Cahn-Hilliard equation with logarithmic potentials. *Milan Journal of Mathematics*, 79(2):561–596, 2011.
- Cohen D.S. and Murray J.D. A generalized diffusion model for growth and dispersal in a population. *Journal of Mathematical Biology*, 12(2):237–249, 1981.
- Cristini V., Li X., Lowengrub J.S., and Wise S.M. Nonlinear simulations of solid tumor growth using a mixture model: invasion and branching. *Journal of Mathematical Biology*, 58(4):723, 2008.
- Eyre D.J. Unconditionally gradient stable time marching the Cahn–Hilliard equation. *MRS Proceedings*, 529:39, 1998.
- Han D. and Wang X. A second order in time, uniquely solvable, unconditionally stable numerical scheme for Cahn-Hilliard–Navier–Stokes equation. *Journal of Computational Physics*, 290:139 – 156, 2015.
- Hanahan D. and Weinberg R.A. Hallmarks of cancer: The next generation. *Cell*, 144(5):646 –

674, 2011.

- Hawkins-Daarud A., van der Zee K.G., and Tinsley Oden J. Numerical simulation of a thermodynamically consistent four-species tumor growth model. *International Journal for Numerical Methods in Biomedical Engineering*, 28(1):3–24, 2012.
- Hecht F. BAMG: Bidimensional anisotropic mesh generator. *INRIA Tech. Report*, 1998.
- Hecht F. New development in FreeFem++. *J. Numer. Math.*, 20(3-4):251–265, 2012.
- Khain E. and Sander L. Generalized Cahn–Hilliard equation for biological applications. *Physical Review. E: Statistical, Nonlinear, and Soft Matter Physics*, 77:051129, 2008.
- Langer J.S. Theory of spinodal decomposition in alloys. *Annals of Physics*, 65(1):53 – 86, 1971.
- Maier-Paape S. and Wanner T. Spinodal decomposition for the cahn-hilliard equation in higher dimensions: Nonlinear dynamics. *Archive for Rational Mechanics and Analysis*, 151(3):187–219, 2000.
- Miranville A. Asymptotic behaviour of a generalized Cahn–Hilliard equation with a proliferation term. *Applicable Analysis*, 92(6):1308–1321, 2013.
- Plapp M. Three-dimensional phase-field simulations of directional solidification. *Journal of Crystal Growth*, 303(1):49 – 57, 2007. ISSN 0022-0248. Proceedings of the Fifth Workshop on Modeling in Crystal Growth.
- Wang Y. and Li J. Phase field modeling of defects and deformation. *Acta Materialia*, 58(4):1212 – 1235, 2010. ISSN 1359-6454.
- Wise S., Lowengrub J., and Cristini V. An adaptive multigrid algorithm for simulating solid tumor growth using mixture models. *Mathematical and Computer Modelling*, 53(1):1 – 20, 2011.
- Wise S.M., Lowengrub J.S., Frieboes H.B., and Cristini V. Three-dimensional multispecies nonlinear tumor growth-I: model and numerical method. *Journal of Theoretical Biology*, 253(3):524–543, 2008.